Geology

Erosional control of the kinematics of the Aconcagua fold-and-thrust belt from numerical simulations and physical experiments

Leonardo Cruz, Julian Malinski, Mia Hernandez, Andrew Take and George Hilley

Geology published online 29 March 2011;
doi: 10.1130/G31675.1

Geology, published online on 29 March 2011 as doi:10.1130/G31675.1

Erosional control of the kinematics of the Aconcagua fold-and-thrust belt from numerical simulations and physical experiments

Leonardo Cruz[1], Julian Malinski[1], Mia Hernandez[1], Andrew Take[2], and George Hilley[1]
[1]Department of Geological and Environmental Sciences, Stanford University, Stanford, California 94305-2115, USA
[2]Department of Civil Engineering, Queen's University, Kingston, Ontario K7L 3N, Canada

ABSTRACT

We investigate the impact of erosion on the geometry and kinematics of the Aconcagua fold-and-thrust belt in central Argentina using analog and numerical models. In these models, the surfaces are eroded according to a rule in which mass removal is limited by the rate of fluvial bedrock incision. This approach unifies principles of frictional failure used in critical Coulomb wedge theory with a quasi-mechanistic erosion rule, which allows us to explicitly relate temporal changes in erosional efficiency in this fold-and-thrust belt to its kinematics. We show that theoretical predictions of the fold-and-thrust belt geometry, as well as the kinematics predicted by both physical and numerical experiments, are both internally consistent and correctly predict the interpreted and measured field geometries. Specifically, the geometric evolution of the Aconcagua fold-and-thrust belt requires relatively high erosion efficiency values (*K*) during the initial stage of deformation, and relatively low *K* values during the latter stages, consistent with the progressive exposure of different rock types during the different stages of deformation. Model results indicate that the activity of the faults in the hinterland is high when erosion is most efficient during the initial stage of deformation; this activity is facilitated by increased out-of-sequence thrusting. In contrast, the models predict that forward-propagating thrusts dominate the latter stages of deformation when erosion is far less efficient. Comparing the geometry of models subjected to erosion with those in which the surface remains uneroded suggests that erosional mass removal is required to explain the geometry of this fold-and-thrust belt. By implication, the results indicate that the kinematics of this, and perhaps other fold-and-thrust belts, may be intimately tied to the temporal history of erosion of the surface topography of these features.

INTRODUCTION

Since the development of the critical Coulomb wedge theory, numerous analytical (e.g., Davis et al., 1983; Dahlen et al., 1984; Dahlen and Suppe, 1988; DeCelles and DeCelles, 2001; Hilley et al., 2004; Hilley and Strecker, 2004; Whipple and Meade, 2004), numerical (e.g., Beaumont et al., 1991, 2001; Willett et al., 1993), analogue (e.g., Cobbold et al. 1993; McClay and Whitehouse, 2004; Konstantinovskaia and Malavieille, 2005; Hoth et al., 2006; Cruz et al., 2007), and field studies or syntheses (e.g., Hodges, 2000; Hilley et al., 2004; Grujic, 2006; Beaumont et al., 2004; Stolar et al., 2006) have suggested that the dynamics of mountain belts may be linked to erosion of Earth's surface. In this process, erosion modifies the distribution of body forces in the crust relative to the case that erosion is absent (e.g., Dahlen and Suppe, 1988). Here we use an erosion rule based on the mass removal expected due to fluvial bedrock incision (e.g., Hilley et al., 2004) implemented for analogue and numerical models (Cruz et al., 2010) to examine the impact that erosion may have on the geometric and kinematic development of a fold-and-thrust belt in central Argentina, the geometric evolution of which is well determined by field observations. We apply this approach to analytical solutions based on the critical Coulomb wedge theory, analogue models of deforming sand wedges, and numerical models of a deforming, strain-weakening frictional orogen scaled to represent the conditions inferred within the fold-and-thrust belt in central Argentina. We examine the consistency between predictions derived from these different modeling approaches and observed field relationships. In this way, we provide a test of the role that erosion plays in the geometric and kinematic development of this mountain belt based on conditions observed or inferred in a real orogen.

FIELD SITE

The geometric and kinematic evolution of the thin-skinned Aconcagua fold-and-thrust belt (AFTB) in the Argentine Andean Cordillera is well constrained by independent geologic methods (e.g., Giambiagi and Ramos, 2002; Ramos et al., 2002). In this orogen, three main tectonic provinces that record the eastward widening of the AFTB have been identified. These tectonic provinces are the Cordillera Principal to the west, the Cordillera Frontal to the east, and the Precordillera farther east (Fig. 1A). The Jurassic–Neogene sedimentary sequence of the Cordillera Principal, which includes evaporites, platform limestones, red beds, mudstones, shales, and siltstones, was actively deforming between ca. 20 and 9 Ma (stage I of deformation). Later, the Cordillera Frontal, which includes pre-Jurassic basement rocks with Neogene sediments, was deformed and uplifted between ca. 9 and 6 Ma (stage II of deformation), and the

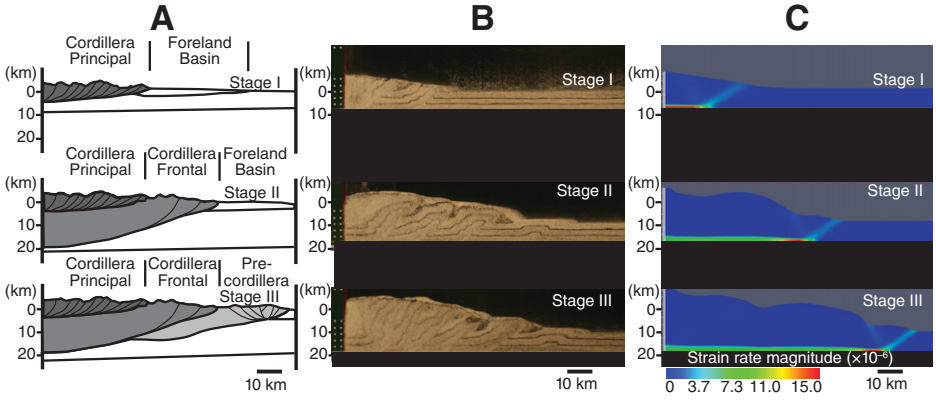

Figure 1. A: Schematic tectonic sections at ~32.5°S depicting three structural provinces of the Aconcagua fold-and-thrust belt (AFTB) including, from west to east, Cordillera Principal, Cordillera Frontal, and Precordillera, and three stages of deformation for AFTB (modified from Hilley et al., 2004). B: Digital photograph of scaled physical experiments of AFTB at final stage of deformation for stages I, II, and III, showing internal deformation, folding and thrusting, and topography in experimental wedges. C: Strain rate magnitude for AFTB Gale numerical simulations showing active thrusts at end of each of the stages. In this study, we used values of erosion efficiency, $K = 1.4 \times 10^{-5}$ m$^{0.2}$/yr, 6.5×10^{-6} m$^{0.2}$/yr, and 6.7×10^{-6} m$^{0.2}$/yr for stages I, II, and III, respectively.

Neogene synorogenic deposits of the Precordillera were uplifted between ca. 5 and 2 Ma (stage III of deformation).

Model-based estimates of the efficiency of erosion have been derived from previous work by comparing simplified semianalytical solutions of the critical Coulomb wedge theory and mass removal due to fluvial bedrock incision (Hilley et al., 2004). During the first stage of deformation, the erosional efficiency required to explain the geometric evolution of the wedge was inferred to be lower than the following two stages, which we interpreted as likely the result of the progressive exposure of more resistant rock types through time in the AFTB. The erosion efficiency values utilized in this study are roughly consistent with the naturally observed range in this value for the types of rocks exhumed during each stage of deformation (Stock and Montgomery, 1999; Hilley et al., 2004).

EXPERIMENTAL AND NUMERICAL APPROACH

The experimental approach and setup were described in detail by Cruz et al. (2010) and the numerical approach is described in the GSA Data Repository.[1] The total thickness of the deformable materials was ~3 cm and was scaled to represent ~8 km of brittle upper crust for stage I, 14 km for stage II, and 16 km for stage III, based on the interpreted detachment depths for each deformation stage (Ramos et al., 2002). Using these lengths, the model was scaled to that of the AFTB (e.g., Hubbert, 1937; Koyi, 1997), including the parameters to calculate erosion rates. This model does not consider rheological heterogeneities in the crust. Deformation during stage I of the AFTB was modeled separately from stages II and III because of the difficulty in experimentally simulating the observed abrupt change in detachment depth between these two sets of stages. However, to assure continuity between the stages, stage II was initiated with a topographic wedge, the geometry of which was scaled to simulate that present at the end of stage I.

The models were deformed and eroded according to the convergence rates and erosion parameters used by Hilley et al. (2004) for the AFTB (summarized in Table DR1 in the Data Repository). We calculated the mass to be removed according to the surface slope observed during the time step and an orogen-scale erosion rule that regards mass removal rates as limited by fluvial bedrock incision according to the following equation, which assumes that changes in the slope of the wedge accommodate the bulk of its volume change (for assessment of this simplification and derivation of this equation, see Cruz et al., 2010):

$$\alpha_2 = \alpha_1 + \operatorname{atan}\left[\left(2\nu T/W^2\right) - \left(2Kk_a^m S^n W^{hm+1}/\mathrm{hm}+1\right)\Delta t\right], \quad (1)$$

where α_1 (L/L) (where L is length) is the initial topographic slope for the given time (t) increment, α_2 (L/L) is the topographic slope after the erosional wave, K ($L^{1-2m}t^{-1}$) is erosion intensity, ka (L^{2-h}) is an area-length coefficient, S (L/L) is the slope of the sand wedge, W (L) is the width of the orogen, T (L) is the thickness of accreted foreland material, v ($L\,t^{-1}$) is the convergence velocity, h is an exponent in area-length relationship, and m and n are the area and slope exponents in the bedrock fluvial incision model (set equal to 0.4 and 1), respectively (Stock and Montgomery, 1999). The erosion time steps were selected according to the time frame of the characteristic step-like growth manifested by the physical experiments and numerical simulations (Cruz et al., 2010).

Numerical models of the deforming sand wedge were carried out using the Gale numerical model (Moresi et al., 2003), using the measured mechanical properties and erosional and boundary conditions identical to those of the sandbox models (see the Data Repository). Gale is an open-source 2-D/3-D (two-dimensional/three-dimensional) software package based on the arbitrary Lagrangian Eulerian (ALE) method used in tectonics problems that solves the Stokes equations on an Eulerian grid and tracks material properties on a Lagrangian grid. We modified the surface-process module in Gale to calculate surface lowering that resulted from the erosion rule used in the experimental sandbox (Cruz et al., 2010). We used a Drucker-Prager failure criterion that is equivalent to a Mohr-Coulomb rheology in two dimensions. To permit the strain localization observed in sandbox experiments, the cohesion of the modeled rheology was allowed to decrease rapidly as strain accrued (Cruz et al., 2010).

RESULTS

We modeled two scenarios of the growth of the AFTB using these different modeling approaches, one in which erosion was prescribed according to the parameters inferred for this area (Table DR1; Hilley et al., 2004), and a base-case scenario in which erosion was absent. When erosion was considered in each of the models at the end of stage I, the widths of the AFTB based on the physical experiment, numerical simulation, and theoretical prediction were 43 km, 41 km, and 38 km, respectively, which compares favorably to the ~50 km width interpreted based on field data (Ramos et al., 2002). The widening rate of the numerical and analogue simulations was initially higher than theoretical predictions at the beginning of stage I due to the initial growth of a wedge of topography in these models that grew subcritically (sensu Dahlen, 1984), rather than by the continuous adjustments required by the theoretical model (Cruz et al., 2010). As documented in our previous work (Cruz et al., 2010), erosion was not applied during this initial phase of subcritical topographic construction. At the end of stage I, ca. 6 Ma, the widths of the physical experiment, numerical simulation, and theoretical prediction were 88 km, 71 km, and 66 km, respectively, while the interpreted AFTB width was 81 km. At the end of stage III ca. 2 Ma, the interpreted width was ~112 km, and the widths of the physical experiment, numerical simulation, and theoretical prediction were 100 km, 104 km, and 108 km, respectively.

In contrast to experiments in which mass was removed from the surface of the modeled fold-and-thrust belt, the final width of the reference noneroding fold-and-thrust belts showed significant differences when compared to the eroding counterparts (Fig. 2). These noneroding models showed widths of 118–120 km at the end of stage I, 150–166 km at the end of stage II, and 193–221 km at the end of stage III, values considerably larger than those produced by the eroding AFTB models and inferred based on observations from the AFTB.

The cumulative shear strain magnitudes derived using particle image velocimetry applied to the physical experiments were similar

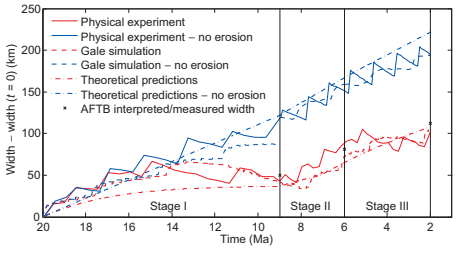

Figure 2. Growth of Aconcagua fold-and-thrust belt (AFTB), including physical experiments (red solid line), Gale numerical simulations (red dashed line), theoretical predictions (red dash-dot line), and observed values (x marks) during three-stage AFTB evolution. Wedge width, defined as distance between rigid backstop and foremost shear band, is plotted versus total displacement of backstop. Plotted wedge width is corrected for width at time, t = 0 to compare models assuming similar initial conditions. Nonerosion reference case is also shown for physical experiments (blue solid line), Gale numerical simulations (blue dashed line), and theoretical predictions (blue dash-dot line).

[1]GSA Data Repository item 2011144, animations for the scaled physical experiments (Videos DR1–DR7) and Gale numerical simulations for the Aconcagua fold-and-thrust belt, is available online at www.geosociety.org/pubs/ft2011.htm, or on request from editing@geosociety.org or Documents Secretary, GSA, P.O. Box 9140, Boulder, CO 80301, USA.

to those produced by numerical simulations at the end of stage I (Figs. 3A and 3B). In particular, the distribution of shear strain and location of shear bands (thrust faults) were similar, and shear strain was localized within shear bands toward the foreland while the highest shear strain magnitudes were diffusely located toward the hinterland of the models. The greater width of shear bands in the numerical simulations, when compared to those in the physical experiments, is responsible for the lower cumulative shear strain observed at a point within the shear bands (i.e., 800% versus 300% for the experimental and numerical simulations, respectively), which, based on our prior work, occurs due to the resolution differences between the two modeling approaches (Cruz et al., 2010). After the final stage of deformation (stage III), the shear strain in the physical and numerical experiments showed clear localization in shear bands in the hinterland and foreland side of the models.

Reference models that were not subjected to erosion showed different kinematics than their eroding counterparts. The cumulative shear strain magnitude in the noneroding fold-and-thrust belt at the end of stage I showed four forward-verging shear bands, while its eroding counterpart showed only two shear bands with strain localized at the back of the wedge (Fig. 3C). At the end of stage III, the reference model showed five shear bands, similar to the eroding AFTB models, but the shear strain magnitude was concentrated in the first and second to last shear bands from the backstop (Fig. 3D).

DISCUSSION

The different modeling approaches presented in this study showed significant similarities among the individual models and correspondence to the interpreted and/or measured AFTB evolving geometries. These models show that the interpreted growth of the AFTB requires relatively efficient erosion to be acting on the fold-and-thrust belt during stage I ($K = 1.4 \times 10^{-5}$ m$^{0.2}$/yr) and that erosional efficiency must decrease ($K = 6.5–6.7 \times 10^{-6}$ m$^{0.2}$/yr) during stages II and III. If the erodibility were held constant and relatively high after stage I, we would expect a significant decrease in the growth rate (Cruz et al., 2010). The variation in erosion efficiency in the AFTB is consistent with the progressive exposure of different types of rocks, including sandstones, mudstones, and platform carbonates with relatively high erodibility during stage I, and metamorphic basement rocks with relatively low erodibility during the later stages of deformation (Ramos et al., 2002; Hilley et al., 2004). This process, where erosional efficiency controls the growth rate of an orogen by lithological variations and/or climate changes, has been proposed for the European Central Alps (e.g., Schlunegger and Simpson, 2002; Willett et al., 2006) and the Central Andes (e.g., McQuarrie et al., 2008) based on geologic observations. In the case of the European Central Alps, this process has been modeled independently with physical (e.g., Bonnet et al., 2007, 2008) and numerical experiments (e.g., Schlunegger and Willett, 1999) with each showing similar results. However, the different model configurations make it difficult to directly compare the modeling results of the different approaches.

Independent analytical solutions of eroding critical Coulomb wedge using different model setups have also shown that erosional efficiency controls orogen widths (e.g., Dahlen and Suppe, 1988; Hilley et al., 2004; Whipple and Meade, 2004) and internal kinematics (Whipple and Meade, 2004), as observed in our models. We argue that this study is the first to provide a rigorous theoretical, analogue, and numerical model intercomparison in an area where the performance of the models can be assessed in the context of field observations of the history of a fold-and-thrust belt. The predictions from the analogue and numerical models in particular compare favorably to one another, suggesting that when rheological properties and boundary conditions are matched, the physics of analogue models can be appropriately simulated using numerical models (e.g., Cruz et al., 2010). More important, all modeling outcomes require that erosion is an integral part of the geometric development of this fold-and-thrust belt, and by inference, the kinematics of this fold-and-thrust belt are likely strongly (and predictably) affected by erosion. In particular, both analogue and numerical models suggest that high erosion rates are associated with localization of shear strain along structures closer to the hinterland of the orogen as activity is sustained for longer periods of time on fewer shear bands (e.g., Merle and Abidi, 1995; Cobbold et al., 1993; Persson and Sokoutis, 2002; Cruz et al., 2010). While this specific model prediction is difficult to test in the AFTB due to a lack of constraints on the activity of individual faults through time along the modeled transect, some degree of increased out-of-sequence thrusting is necessary to produce the observed limited wedge propagation during stage I. Likewise, a decrease in the total slip along individual faults and an increased number of forward-propagating faults appear necessary to facilitate the increased frontal propagation rate observed in the AFTB during stages II and III. Thus, it appears likely that erosion plays a crucial role in determining both the geometry and kinematics of the AFTB and, by implication, may play a similar role in other mountain belts.

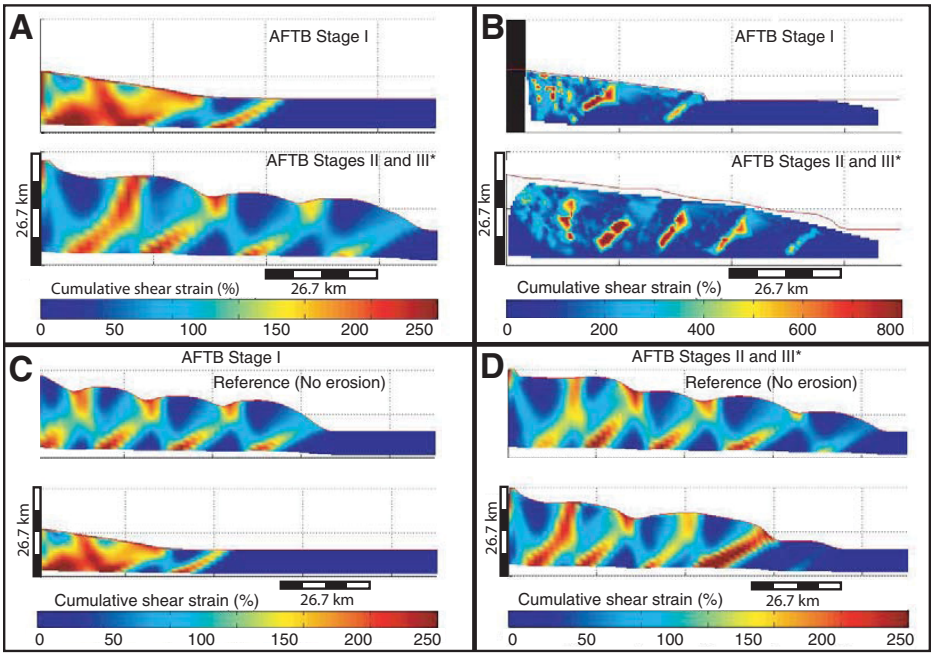

Figure 3. Aconcagua fold-and-thrust belt (AFTB) cumulative shear strain. A: Calculated for Gale numerical simulations. B: Calculated for scaled physical experiments. Asterisk indicates that the strain analysis for final stage (III) in both physical experiments and Gale simulations for A and B only includes 80% of total displacement accrued during this stage due to particle image velocimetry constraints during physical experiment analysis. C: Cumulative shear strain calculated for Gale numerical simulations of (bottom) eroding AFTB scenario and (top) reference nonerosion simulation for stage I. D: Same as C, except that accretion and erosion parameters for stages II and III were used. Erosion of wedge surface concentrates deformation along fewer shear bands in simulated AFTB when compared to nonerosion reference simulation.

The rock trajectories observed in our experimental results are qualitatively similar to those presented by Dahlen and Barr (1989). Experiments and analytical solutions both show enhanced vertical flow in the back of the wedge driven by erosion. This is only a first-order comparison because our experiments have not been subjected to deformation and erosion long enough to obtain the steady state between accretion and erosion that is assumed in the analytical solutions. However, these results indicate that analytic solutions may provide broad insight into tectonic-erosion interactions, but may be problematic when considering local kinematics.

ACKNOWLEDGMENTS

This research was supported by National Science Foundation grant EAR-0711185. We thank Walter Landry at the Computational Infrastructure for Geodynamics (CIG) for his support during the implementation of the surface process module in the Gale code. We appreciate careful reviews by Todd Ehlers and two anonymous reviewers that improved this manuscript.

REFERENCES CITED

Beaumont, C., Fullsack, P., and Hamilton, J., 1991, Erosional control of active compressional orogens, *in* McClay, K.R., ed., Thrust tectonics: New York, Chapman and Hall, p. 1–18.

Beaumont, C., Jamieson, R.A., Nguyen, M.H., and Lee, B., 2001, Himalayan tectonics explained by extrusion of a low-viscosity crustal channel coupled to focused surface denudation: Nature, v. 414, p. 738–742, doi: 10.1038/414738a.

Beaumont, C., Jamieson, R.A., Nguyen, M.H., and Medvedev, S., 2004, Crustal channel flows: 1. Numerical models with applications to the tectonics of the Himalayan-Tibetan orogen: Journal of Geophysical Research, v. 109, B06406, doi: 10.1029/2003JB002809.

Bonnet, C., Malavielle, J., and Mosar, J., 2007, Interactions between tectonics, erosion, and sedimentation during the recent evolution of the Alpine orogen: Analogue modeling insights: Tectonics, v. 26, TC6016, doi: 10.1029/2006TC002048.

Bonnet, C., Malavieille, J., and Mosar, J., 2008, Surface processes versus kinematics of thrust belts: Impact on rates of erosion, sedimentation, and exhumation—Insights from analogue models: Bulletin de la Société Géologique de France, v. 179, p. 297–314.

Cobbold, P.R., Davy, P., Gapais, D., Rossello, E.A., Sadybakasov, E., Thomas, J.C., Tondji Biyo, J.J., and de Urreiztieta, M., 1993, Sedimentary basins and crustal thickening: Sedimentary Geology, v. 86, p. 77–89, doi: 10.1016/0037-0738(93)90134-Q.

Cruz, L., Teyssier, C., Perg, L., Take, A., and Fayon, A., 2007, Deformation, exhumation, and topography of experimental doubly-vergent orogenic wedges subjected to asymmetric erosion: Journal of Structural Geology, v. 30, p. 98–115, doi: 10.1016/j.jsg.2007.10.003.

Cruz, L., Malinski, J., Wilson, A., Take, A., and Hilley, G., 2010, Erosional control of the kinematics and geometry of fold-and-thrust belts imaged in a physical and numerical sandbox: Journal of Geophysical Research, v. 115, B09404, doi: 10.1029/2010JB007472.

Dahlen, F.A., 1984, Noncohesive critical Coulomb wedges: An exact solution: Journal of Geophysical Research, v. 89, p. 10,125–10,133, doi: 10.1029/JB089iB12p10125.

Dahlen, F.A., and Barr, T.E., 1989, Brittle frictional mountain building, 1. Deformation and mechanical energy budget: Journal of Geophysical Research, v. 94, p. 3906–3922, doi: 10.1029/JB094iB04p03906.

Dahlen, F.A., and Suppe, J., 1988, Mechanics, growth, and erosion of mountain belts, *in* Clark, S.P., et al., eds., Processes in continental lithospheric deformation: Geological Society of America Special Paper 218, p. 161–178.

Dahlen, F.A., Suppe, J., and Davis, D., 1984, Mechanics of fold-and-thrust belts and accretionary wedges: Cohesive Coulomb theory: Journal of Geophysical Research, v. 89, p. 10,087–10,101, doi: 10.1029/JB089iB12p10087.

Davis, D., Suppe, J., and Dahlen, F.A., 1983, Mechanics of fold-and-thrust belts and accretionary wedges: Journal of Geophysical Research, v. 88, p. 1153–1172, doi: 10.1029/JB088iB02p01153.

DeCelles, P.G., and DeCelles, P.C., 2001, Rates of shortening, propagation, underthrusting, and flexural wave migration in continental orogenic systems: Geology, v. 29, p. 135–138, doi: 10.1130/0091-7613(2001)029<0135:ROSPUA>2.0.CO;2.

Giambiagi, L.B., and Ramos, P.C., 2002, Structural evolution of the Andes in a transitional zone between flat and normal subduction (33°300–33°450s), Argentina and Chile: Journal of South American Earth Sciences, v. 15, p. 101–116, doi: 10.1016/S0895-9811(02)00008-1.

Grujic, D., 2006, Climatic forcing of erosion, landscape, and tectonics in the Bhutan Himalayas: Geology, v. 34, p. 801–804, doi: 10.1130/G22648.1.

Hilley, G.E., and Strecker, M.R., 2004, Steady-state erosion of critical Coulomb wedges with applications to Taiwan and the Himalaya: Journal of Geophysical Research, v. 109, B01411, doi: 10.1029/2002JB002284.

Hilley, G.E., Strecker, M.R., and Ramos, V.A., 2004, Growth and erosion of fold-and-thrust belts with an application to the Aconcagua fold-and-thrust belt, Argentina: Journal of Geophysical Research, v. 109, B01410, doi: 10.1029/2002JB002282.

Hodges, K.V., 2000, Tectonics of the Himalaya and southern Tibet from two perspectives: Geological Society of America Bulletin, v. 112, p. 324–350, doi: 10.1130/0016-7606(2000)112<324:TOTHAS>2.0.CO;2.

Hoth, S., Adam, J., Kukowski, N., and Oncken, O., 2006, Influence of erosion on the kinematics of bivergent orogens; results from scaled sandbox simulations, *in* Willett, S.D., et al., eds., Tectonics, climate, and landscape evolution: Geological Society of America Special Paper 398, p. 201–225, doi: 10.1130/2006.2398(12).

Hubbert, M.K., 1937, Theory of scale models as applied to the study of geologic structures: Geological Society of America Bulletin, v. 48, p. 1459–1520.

Konstantinovskaia, E., and Malavieille, J., 2005, Erosion and exhumation in accretionary orogens: Experimental and geological approaches: Geochemistry Geophysics Geosystems, v. 6, Q02006, doi: 10.1029/2004GC000794.

Koyi, H., 1997, Analogue modeling: From a qualitative to a quantitative technique: A historical outline: Journal of Petroleum Geology, v. 20, p. 223–238, doi: 10.1111/j.1747-5457.1997.tb00774.x.

McClay, K.R., and Whitehouse, P.S., 2004, Analog modeling of doubly vergent thrust wedges, *in* McClay, K.R., ed., Thrust tectonics and hydrocarbon systems: American Association of Petroleum Geologists Memoir 82, p. 184–206.

McQuarrie, N., Ehlers, T., Barnes, J., and Meade, B., 2008, Temporal variation in climate and tectonic coupling in the central Andes: Geology, v. 36, p. 999–1002, doi: 10.1130/G25124A.1.

Merle, O., and Abidi, N., 1995, Approche expérimentale du fonctionnement des rampes émergentes: Bulletin de la Société Géologique de France, v. 166, p. 439–450.

Moresi, L.N., Dufour, F., and Mühlhaus, H.-B., 2003, A Lagrangian integration point finite element method for large deformation modeling of viscoelastic geomaterials: Journal of Computational Physics, v. 184, p. 476–497, doi: 10.1016/S0021-9991(02)00031-1.

Persson, K.S., and Sokoutis, D., 2002, Analogue models of orogenic wedges controlled by erosion: Tectonophysics, v. 356, p. 323–336, doi: 10.1016/S0040-1951(02)00443-2.

Ramos, V.A., Cristallini, E.O., and Perez, D.J., 2002, The Pampean flat-slab of the central Andes: Journal of South American Earth Sciences, v. 15, p. 59–78, doi: 10.1016/S0895-9811(02)00006-8.

Schlunegger, F., and Willett, S.D., 1999, Spatial and temporal variations in exhumation of the Central Swiss Alps and implications for exhumation mechanisms, *in* Brandon, M., and Willett, S.D., eds., Exhumation processes: normal faulting, ductile flow, and erosion: Geological Society of London Special Publication 154, p. 157–180.

Schlunegger, F., and Simpson, G., 2002, Possible erosional control on lateral growth of the European Central Alps: Geology, v. 30, p. 907–910, doi: 10.1130/0091-7613(2002)030<0907:PECOLG>2.0.CO;2.

Stock, J.D., and Montgomery, D.R., 1999, Geologic constraints on bedrock river incision using the stream power law: Journal of Geophysical Research, v. 104, no. B3, p. 983–993, doi: 10.1029/98JB02139.

Stolar, D.R., Willett, S.D., and Roe, G.H., 2006, Climatic and tectonic forcing of a critical orogen, *in* Willett, S.D., et al., eds., Tectonics, climate, and landscape evolution: Geological Society of America Special Paper 398, p. 241–250, doi: 10.1130/2006.2398(14).

Whipple, K.X, and Meade, B.J., 2004, Controls on the strength of coupling among climate, erosion, and deformation in two-sided, frictional orogenic wedges at steady state: Journal of Geophysical Research, v. 109, p. 1–24, doi: 10.1029/2003JF000019.

Willett, S., Beaumont, C., and Fullsack, P., 1993, Mechanical model for the tectonics of doubly vergent compressional orogens: Geology, v. 21, p. 371–374, doi: 10.1130/0091-7613(1993)021<0371:MMFTTO>2.3.CO;2.

Willett, S., Schlunegger, F., and Picotti, V., 2006, Messinian climate change and erosional destruction of the central European Alps: Geology, v. 34, p. 613–616, doi: 10.1130/G22280.1.

Manuscript received 18 August 2010
Revised manuscript received 2 December 2010
Manuscript accepted 12 December 2010

Printed in USA